

## Reflection Tomographic Imaging of Highly Scattering Objects Using Incremental Frequency Inversion

Kadu, A.; Mansour, H.; Boufounos, P.T.; Liu, D.

TR2019-012 March 29, 2019

### Abstract

Reflection tomography is an inverse scattering technique that estimates the spatial distribution of an object's permittivity by illuminating it with a probing pulse and measuring the scattered wavefields by receivers located on the same side as the transmitter. Unlike conventional transmission tomography, the reflection regime is severely ill-posed since the measured wavefields contain far less spatial frequency information about the object. In this paper, we propose an incremental frequency inversion framework that requires no initial target model, and that leverages spatial regularization to reconstruct the permittivity distribution of highly scattering objects. Our framework solves a wave-equation constrained, total-variation (TV) regularized nonlinear least squares problem that solves a sequence of subproblems that incrementally enhance the resolution of the estimated object model. With each subproblem, higher frequency wavefield components are incorporated in the inversion to improve the recovered model resolution. We validate the performance of our approach using synthetically generated data for retrieving high-contrast material such as water in an underground radar imaging setup

*IEEE International Conference on Acoustics, Speech, and Signal Processing (ICASSP)*

This work may not be copied or reproduced in whole or in part for any commercial purpose. Permission to copy in whole or in part without payment of fee is granted for nonprofit educational and research purposes provided that all such whole or partial copies include the following: a notice that such copying is by permission of Mitsubishi Electric Research Laboratories, Inc.; an acknowledgment of the authors and individual contributions to the work; and all applicable portions of the copyright notice. Copying, reproduction, or republishing for any other purpose shall require a license with payment of fee to Mitsubishi Electric Research Laboratories, Inc. All rights reserved.



# REFLECTION TOMOGRAPHIC IMAGING OF HIGHLY SCATTERING OBJECTS USING INCREMENTAL FREQUENCY INVERSION

Ajinkya Kadu\*

Hassan Mansour, Petros T. Boufounos, Dehong Liu

Mathematical Institute, Utrecht University  
Utrecht 3584 CD, The Netherlands  
a.a.kadu@uu.nl

Mitsubishi Electric Research Laboratories  
Cambridge, MA 02139, USA  
{mansour, petrosb, liudh}@merl.com

## ABSTRACT

Reflection tomography is an inverse scattering technique that estimates the spatial distribution of an object's permittivity by illuminating it with a probing pulse and measuring the scattered wavefields by receivers located on the same side as the transmitter. Unlike conventional transmission tomography, the reflection regime is severely ill-posed since the measured wavefields contain far less spatial frequency information about the object. In this paper, we propose an incremental frequency inversion framework that requires no initial target model, and that leverages spatial regularization to reconstruct the permittivity distribution of highly scattering objects. Our framework solves a wave-equation constrained, total-variation (TV) regularized nonlinear least squares problem that solves a sequence of subproblems that incrementally enhance the resolution of the estimated object model. With each subproblem, higher frequency wavefield components are incorporated in the inversion to improve the recovered model resolution. We validate the performance of our approach using synthetically generated data for retrieving high-contrast material such as water in an underground radar imaging setup.

**Index Terms**— Computational imaging, inverse scattering, total variation regularization, alternating direction method of multipliers

## 1. INTRODUCTION

Inverse scattering deals with the problem of reconstructing an image of the spatial permittivity of an object by probing it using electromagnetic or acoustic waves of finite bandwidth and measuring the scattered wavefield around the object. An incident wavefield propagating inside the object induces multiple scattering waves that are generally measured on the boundary of the material. Consequently, the scattered waves contain information about the spatial distribution of the material properties, which has led to applications in numerous fields, such as, non-destructive testing [1], optical tomography [2], geophysical imaging [3], ground penetrating radar [4], and medical imaging [5].

Two main acquisition modes exist in inverse scattering: (i) transmission mode, where the transmitters and receivers are located on opposite sides of the material; (ii) reflection mode, where the transmitters and receivers are located on the same side of the object. The reflection setup generally arises due to a limitation to accessing only one side of the material, as in the case of underground imaging, illustrated in Figure 1. We focus our presentation on the reflection tomography scenario where the problem is severely

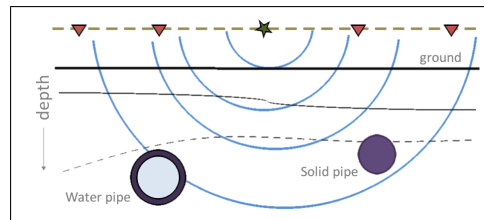


**Fig. 1:** Acquisition scenario for underground imaging. Green  $\star$  denotes the source and red  $\nabla$  denotes the receivers.

ill-posed. This scenario often arises in underground imaging applications such as ground penetrating radar and seismic imaging.

Numerous techniques have been proposed for solving the inverse scattering problem in the reflection regime. Earlier approaches dealt with iteratively linearizing the scattering model, using straight ray theory, Born approximation, Rytov approximation, and reverse-time migration [6, 7, 8, 9]. However, such linear models fail to account for the complex interaction between the wavefield and the material properties that result in multiple scattering. As a result, these methods require an accurate initial target model to enable the inversion and generally suffer from poor reconstruction quality especially when the material is inhomogeneous or contains highly scattering objects. Recently, the nonlinear interaction between the wavefield and the material has been incorporated into the inversion process using the wave equation [10]. The inverse problem that deals with the wave-equation based scattering model is known as full-waveform inversion (FWI) [11, 12, 13]. This approach has been utilized for diffraction tomography [14, 15]. More recently, learning approaches have been proposed to solve such scattering model [16, 17].

In this paper, we develop an incremental frequency inversion framework that poses the underground imaging problem as a sequence of constrained nonlinear least-squares subproblems. With each new subproblem, higher frequency wavefield components are included in the data-misfit function, thereby regularizing the solution of the new subproblem to remain consistent with the lower frequency measurements. The nonlinear interaction between the wavefield and the medium is accurately modeled through a wave-equation constraint. Moreover, the recovered solution is further regularized through a bounded total-variation penalty function. We describe in Section 2 the formulation of the forward and inverse problems and discuss the additional challenges of solving the reflection tomography problem. In Section 3, we present the details of our incremental frequency inversion framework and validate the performance of our proposed approach in Section 4.

\*This work was conducted while Ajinkya Kadu was an intern at MERL.

## 2. PROBLEM FORMULATION

We begin by presenting the scattering model that describes the relation between the scattered wavefield and the medium parameters. Next, we formulate the discrete inverse problem to reconstruct the medium from the set of measured scattered wavefield. Finally, we discuss some challenges in estimating the material properties of an object in the reflection regime.

### 2.1. Forward problem

A wave-equation governs the acoustic or electromagnetic scattering from an inhomogeneous medium in the time domain. An equivalent representation in the frequency domain is the scalar Helmholtz equation. In this work, we focus on the integral form of the Helmholtz equation, known as the scalar Lippmann-Schwinger equation. Let  $u_{sc} : \Omega \rightarrow \mathbb{C}$  be the scattered wavefield inside a spatial domain, or region of interest,  $\Omega$ , let  $f : \Omega \rightarrow \mathbb{R}$  be the medium parameters and denote by  $g : \Omega \rightarrow \mathbb{C}$  the free-space Green's function. The scalar Lippmann-Schwinger scattering equation is then defined as follows

$$u_{sc}(\mathbf{x}) = u_{in}(\mathbf{x}) + k^2 \int_{\Omega} g(\mathbf{x} - \mathbf{r}) u_{sc}(\mathbf{r}) f(\mathbf{r}) d\mathbf{r}, \quad \forall \mathbf{x} \in \Omega \quad (1)$$

where,  $u_{in}$  is the input wavefield generated by the transmitter, and  $k = 2\pi/\lambda$  is the wavenumber with  $\lambda$  denoting the wavelength. The medium parameters,  $f(\mathbf{x}) = (\epsilon(\mathbf{x}) - \epsilon_b)$ , is the relative permittivity, where  $\epsilon(\mathbf{x})$  is the permittivity of the object and  $\epsilon_b$  is the permittivity of the background, which is assumed to be the vacuum ( $\epsilon_{vacuum} = 1$ ). The free-space Green's function for the Helmholtz equation ( $\nabla^2 + k^2$ )  $g = \delta$  is given by:

$$g(\mathbf{x}) \triangleq \begin{cases} -\frac{i}{2k} e^{-ikr} & d = 1 \\ -\frac{i}{4} H_0^{(2)}(kr) & d = 2, \\ \frac{1}{4\pi r} e^{-ikr} & d = 3 \end{cases}$$

where  $r = \|\mathbf{x}\|$ ,  $H_0^{(2)}$  is the zero-order Hankel function of second kind, and  $d$  is the dimension of  $\Omega$ . The scattered wavefield is then measured at the receivers resulting in the following data equation:

$$y(\mathbf{x}) = \int_{\Omega} h(\mathbf{x} - \mathbf{r}) f(\mathbf{r}) u_{sc}(\mathbf{r}) d\mathbf{r}, \quad \forall \mathbf{x} \in \Gamma, \quad (2)$$

where  $h : \Omega \rightarrow \mathbb{C}$  denotes the Green's function of the receiver and  $\Gamma$  is the receiver domain. The forward problem involves computing  $y$  given the input wavefield  $u_{in}$ , medium parameters  $f$ , and the Green's functions  $g$  and  $h$ .

In the discrete setting, the scattering equation and data equation reduce to the following system of linear equations for each transmitter illumination and wave number:

$$\begin{aligned} \mathbf{u} &= \mathbf{v} + \mathbf{G} \mathbf{diag}(\mathbf{f}) \mathbf{u}, \\ \mathbf{y} &= \mathbf{H} \mathbf{diag}(\mathbf{f}) \mathbf{u}, \end{aligned} \quad (3)$$

where  $\mathbf{u} \in \mathbb{C}^N$  and  $\mathbf{v} \in \mathbb{C}^N$  are the scattered and input wavefields, respectively,  $N$  denotes the number of gridpoints used to discretize the domain  $\Omega$ ,  $\mathbf{f} \in \mathbb{R}^N$  denotes the medium parameters, while  $\mathbf{G} \in \mathbb{C}^{N \times N}$  and  $\mathbf{H} \in \mathbb{C}^{n_{rec} \times N}$  are the Green's functions of the domain and receivers, respectively. Let  $n_{rec}$  be the number of receivers that discretizes the receiver domain  $\Gamma$ , then  $\mathbf{y} \in \mathbb{C}^{n_{rec}}$  is the noise-free scattered wavefield measured at the receivers. The

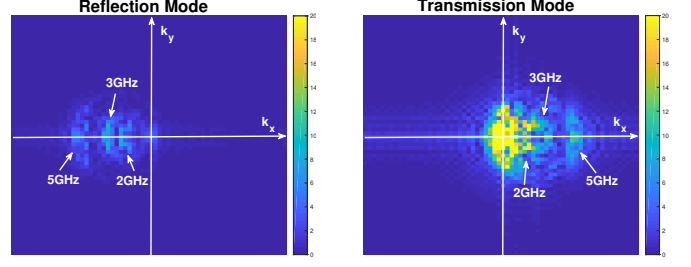


**Fig. 2:** Comparison of the spatial frequency content of the received wavefields between the transmission mode and the reflection mode from a transmitted pulse containing 2GHz, 3GHz, and 5GHz frequency components.

critical step in the forward problem involves estimating the scattered wavefield  $\mathbf{u}$  by inverting the matrix  $\mathbf{A} := \mathbf{I} - \mathbf{G} \mathbf{diag}(\mathbf{f})$ , where  $\mathbf{I}$  denotes the identity operator. As the discretization dimension  $N$  increases, explicitly forming the matrix  $\mathbf{A}$  and its inverse becomes prohibitively expensive. Therefore, a functional form of  $A$  along with the conjugate-gradient method (CG) are often used to perform the inversion. We note here that the convergence of CG depends on the conditioning of the operator  $\mathbf{A}$ , which become ill-conditioned for large wavenumber and highly scattering medium, *i.e.*, large value of  $\|\mathbf{f}\|_{\infty}$ .

### 2.2. Inverse problem

An inverse scattering problem is defined as the estimation of medium parameters given the measurement of scattered wavefield at  $n_{rec}$  receivers for each input wavefield generated from  $n_t$  transmitters. In the discrete setting and assuming that measurements are contaminated by white Gaussian noise, we can formulate inverse problem as follows:

$$\begin{aligned} \min_{\mathbf{f}, \mathbf{u}} \quad & \sum_{j=1}^{n_f} \sum_{i=1}^{n_t} \frac{1}{2} \|\mathbf{y}_{ij} - \mathbf{H}_j \mathbf{diag}(\mathbf{f}) \mathbf{u}_{ij}\|_2^2, \\ \text{s.t.} \quad & (\mathbf{I} - \mathbf{G}_j \mathbf{diag}(\mathbf{f})) \mathbf{u}_{ij} = \mathbf{v}_{ij} \quad \forall i, j, \end{aligned} \quad (4)$$

where  $n_f$  are the number of frequencies, and  $\mathbf{y}_{ij}$  is the noisy data received at  $n_{rec}$  receivers from transmitter  $i$  at frequency  $j$ .

Let  $\Pi = \{\mathbf{f}^*, \mathbf{u}^*\}$  denote the solution set of the problem (4). In general, problem (4) is ill-posed and admits multiple solutions, *i.e.*,  $|\Pi| > 1$ . Therefore, spatial regularization in the form of a penalty function  $\mathcal{R}(\mathbf{f})$  is often added to reduce the solution space. The regularized problem is then represented as

$$\begin{aligned} \min_{\mathbf{f}, \mathbf{u}} \quad & \sum_{i,j} \mathcal{D}_{ij}(\mathbf{f}, \mathbf{u}_{ij}) + \mathcal{R}(\mathbf{f}), \\ \text{s.t.} \quad & (\mathbf{I} - \mathbf{G}_j \mathbf{diag}(\mathbf{f})) \mathbf{u}_{ij} = \mathbf{v}_{ij} \quad \forall i, j, \end{aligned} \quad (5)$$

where,  $\mathcal{D}_{ij}$  represents the data-fidelity term for transmitter  $i$  at frequency  $j$ .

### 2.3. Inversion challenges in the reflection regime

A critical distinction between the transmission and reflection modes in inverse scattering manifests itself in the amount of spatial frequency content that can be captured by the measured wavefields. In the transmission regime, the received measurements generally capture more of the lower spatial frequencies of the target

distribution compared to the reflection regime. We illustrate this fact by plotting in Figure 2 the spatial frequency content of the received wavefields of a target illuminated from the left side by a flat spectrum pulse containing 2GHz, 3GHz, and 5GHz frequency components. We compute the spatial frequency content in each case by solving (4) for  $\mathbf{f}$  while providing the true scattered wavefields  $\mathbf{u}_{ij}^* = (\mathbf{I} - \mathbf{G}_j \text{diag}(\mathbf{f}^{\text{true}}))^{-1} \mathbf{v}_{ij}$  for each frequency. Notice how the reflection mode exhibits very little energy around the low spatial frequency subbands in the Fourier plane. This is in stark contrast to the transmission mode where a significant portion of the received signal energy corresponds to the low spatial frequencies.

### 3. PROPOSED METHOD

In this section, we present an incremental frequency inversion method that does not require a smooth initial model of the target image for successful recovery.

#### 3.1. Frequency Separation

The least-squares cost function in (5) provides a natural separation across frequencies. Moreover, the topology of the nonconvex cost function varies drastically between frequencies and can be leveraged to find good local minima. We illustrate this behavior using a simple cylindrical model for the target with a constant reflectivity  $c$  as shown in Figure 3(a). The true target has a reflectivity  $c = 100$  and is illuminated with transmitters located at  $-0.6\text{m}$   $y$ -position. We plot in Figure 3(b) the value of the data-fidelity cost function  $\sum_{j=1}^k \sum_{i=1}^{n_i} \mathcal{D}_{ij}(\mathbf{f}, \mathbf{u}_{ij})$ , where  $k$  varies from the 10 MHz index to the 50 MHz index, and where the reflectivity  $c$  ranges from 0 to 120. Notice that as higher frequency wavefields are introduced, the cost function starts to exhibit many local minima that are farther away from the global minimizer compared to the low-frequency wavefields.

The observations above led us to propose an incremental frequency inversion framework where the model of the object's permittivity is sequentially updated as higher frequencies are included in the inversion. Given a measured wavefield containing  $n_f$  frequency components indexed in increasing order from 1 to  $n_f$ , our framework iteratively estimates the model from low to high-frequency while keeping the low-frequency cost function as a regularizer for high-frequency inversions:

for  $k = 1, \dots, n_f$ :

$$\left( \mathbf{f}^k, \mathbf{u}^* \right) \triangleq \underset{\mathbf{f}, \mathbf{u}}{\text{argmin}} \left\{ \mathcal{D}_k(\mathbf{f}, \mathbf{u}_k) + \sum_{j=1}^{k-1} \lambda_j \mathcal{D}_j(\mathbf{f}, \mathbf{u}_j) + \mathcal{R}(\mathbf{f}) \right. \\ \left. \text{s.t. } (\mathbf{I} - \mathbf{G}_j \text{diag}(\mathbf{f})) \mathbf{u}_{ij} = \mathbf{v}_{ij} \forall i, j \right\}, \quad (6)$$

where  $\mathcal{D}_j(\mathbf{f}, \mathbf{u}_j) = \sum_{i=1}^{n_i} \mathcal{D}_{ij}(\mathbf{f}, \mathbf{u}_{ij})$ , and  $\lambda_j \in (0, 1]$  are regularization parameters that control the impact of the low-frequencies cost functions with respect to the  $k^{\text{th}}$ -frequency cost function. Therefore, instead of solving a single nonconvex minimization problem in (5), we solve  $n_f$  subproblems sequentially according to (6), where the sequence of solutions moves us closer to the global minimizer of (5).

To solve the minimization problem in (6), we use a proximal Quasi-Newton method [18]. We first compute the gradient of the

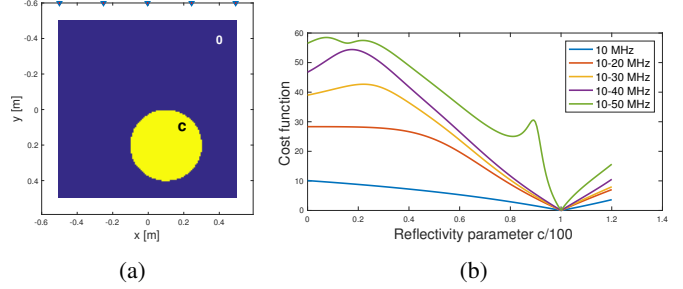


**Fig. 3:** (a) Illustration of a cylindrical object with true reflectivity equal to  $c = 100$  measured by five co-located transmitters and receivers. (b) Topology of the cost function on the frequency content of the wavefield relative to the estimated reflectivity  $c$  as it varies from 0 to 120.

$$\mathcal{F}(\mathbf{f}, \mathbf{u}) \triangleq \mathcal{D}_k(\mathbf{f}, \mathbf{u}_k) + \sum_{j=1}^{k-1} \lambda_j \mathcal{D}_j(\mathbf{f}, \mathbf{u}_j)$$

with respect to  $\mathbf{f}$ , with the wavefield  $\mathbf{u}$  satisfying the PDE constraints. Such gradient computation is performed using an adjoint-state method [19]. A descent direction is then obtained by forming an approximation to the Hessian using limited memory BFGS [20]. A  $(t+1)^{\text{th}}$ -iterate of the model is then given by

$$\mathbf{f}^{(t+1)} \triangleq \mathcal{P}_{TV \leq \tau} \left( \mathbf{f}^{(t)} - \gamma_t \tilde{\mathbf{H}}^{-1} \nabla_{\mathbf{f}} \mathcal{F}(\mathbf{f}^{(t)}, \mathbf{u}) \right),$$

where  $\gamma_t$  is a step length computed using backtracking line-search [21],  $\tilde{\mathbf{H}}$  is an L-BFGS Hessian, and  $\mathcal{P}_{TV \leq \tau}(\cdot)$  is a proximal operator for the TV-norm constrained by  $\tau$ . For each frequency batch in (6), we keep updating the model till the norm of the gradient diminishes to a small value.

---

#### Algorithm 1 Proximal for constrained TV regularization

---

**Input:**  $\mathbf{w} \in \mathbb{R}^n, \mathbf{D} \in \mathbb{R}^{m \times n}, \tau > 0, \rho > 0, t_{\max}, \gamma \in (0, 1]$

**Output:**  $\mathbf{f}^{(t_{\max})}$

- 1:  $\mathbf{f}^{(0)} = \mathbf{w}^{(k)}, \mathbf{z}^{(0)} = \mathbf{0}, \lambda^{(0)} = \mathbf{0}$
  - 2: **for**  $t = 0$  to  $t_{\max}$  **do**
  - 3:  $\mathbf{f}^{(t+1)} := (\mathbf{I} - \rho \mathbf{D}^T \mathbf{D})^{-1} (\mathbf{w} + \mathbf{D}^T (\mathbf{z}^{(t)} - \lambda^{(t)}))$
  - 4:  $\mathbf{z}^{(t+1)} := \mathcal{P}_{\|\cdot\|_1 \leq \tau} (\mathbf{D} \mathbf{f}^{(t+1)} + \lambda^{(t+1)})$
  - 5:  $\lambda^{(t+1)} := \lambda^{(t)} + \gamma (\mathbf{D} \mathbf{f}^{(t+1)} - \mathbf{z}^{(t+1)})$
  - 6: check termination conditions
  - 7: **end for**
  - 8: **return**  $\mathbf{f}^{(t_{\max})}$
- 

#### 3.2. Total-Variation Regularization

Formally, the Total-Variation(TV) norm for a function  $u : \Omega \rightarrow \mathbb{R}$  is represented with the help of bounded function  $\phi$  as

$$TV(u) \triangleq \sup \left\{ \int_{\Omega} u(\mathbf{x}) \text{div} \phi \, d\mathbf{x} : \phi \in \mathcal{C}_c^1(\Omega, \mathbb{R}^d), \|\phi\|_{\infty} \leq 1 \right\}, \\ = \int_{\Omega} |\nabla u(\mathbf{x})| \, d\mathbf{x} = \|\nabla u(\mathbf{x})\|_1.$$

This norm measures the total change in the derivative of the function over a finite domain [23]. As a result, regularization with a TV norm

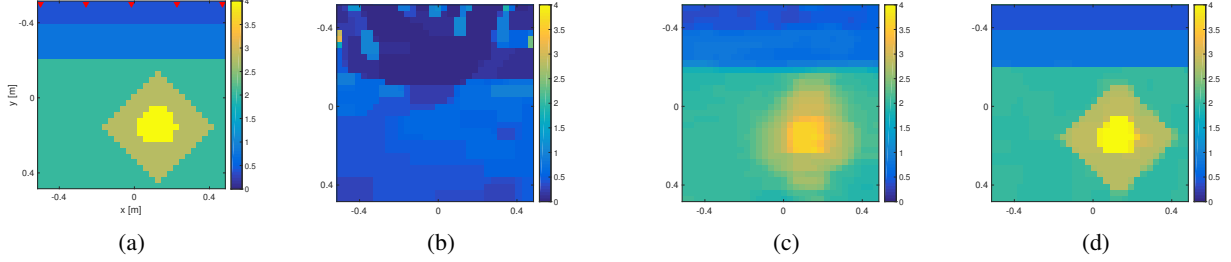


**Fig. 4:** Comparison of the reconstruction quality of the scene shown in (a), between (b) the combined frequency setup of [14], (c) the one frequency at a time setup of [22], and (d) our proposed incremental frequency inversion setup.

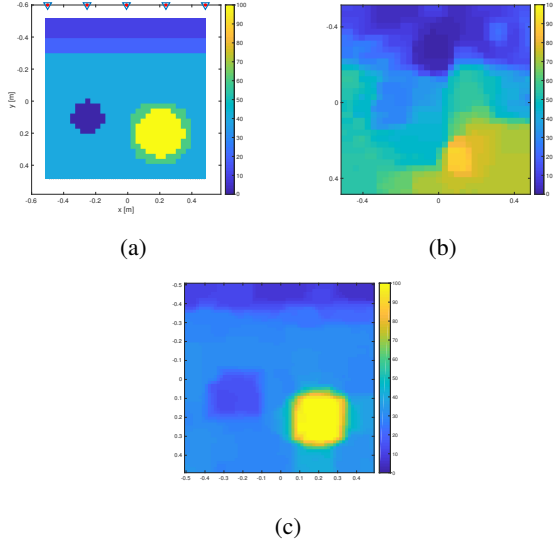


**Fig. 5:** (a) Simulated underground scene; (b) reconstruction with the one frequency at a time setup of [22]; (c) and our proposed incremental frequency inversion method.

promotes piecewise constant approximation of the true model [24]. We adopt the TV regularization in its constrained form, such that,

$$\mathcal{R}_{TV}(\mathbf{f}) \triangleq \delta(TV(\mathbf{f}) \leq \tau), \quad (7)$$

where  $\delta(\cdot)$  is an indicator function, and  $\tau$  is a constraint parameter. Let  $\mathbf{D}$  be the finite difference operator that discretizes the gradient, then  $TV(\mathbf{f}) = \|\mathbf{D}\mathbf{f}\|_1$ .

In order to impose the TV norm constraint, we define the proximal operator:

$$\mathcal{P}_{TV \leq \tau}(\mathbf{w}) \triangleq \underset{\mathbf{f}}{\operatorname{argmin}} \left\{ \frac{1}{2} \|\mathbf{f} - \mathbf{w}\|_2^2 + \mathcal{R}_{TV}(\mathbf{f}) \right\} \quad (8)$$

which can be evaluated using the alternating direction method of multipliers (ADMM) [25], as shown in Algorithm 1. The projection onto the  $\ell_1$  norm described in the step 4 is performed explicitly using the algorithm described in [26].

#### 4. NUMERICAL EXPERIMENT

In order to evaluate the performance of our proposed method, we generate two synthetic underground models with relatively large contrast variation in the object permittivity. In the first experiment, we consider the underground scene, shown in Figure 4(a), where maximum permittivity is set to 4. We illuminate the scene with a flat spectrum pulse occupying the frequency band [100, 800] MHz with a 100 MHz step. The domain is discretized to a  $32 \times 32$  grid

to cover a  $1\text{m} \times 1\text{m}$  area. We compare the recovery performance of our proposed approach in Figure 4(d) to the combined frequency approach of [14, 15] in Figure 4(b), and to the sequential one frequency at a time approach originally proposed in [12] and since then refined in numerous publications including [22] in Figure 4(c) with the added modification of incorporating the TV regularization. In the noise-free setting, our method achieves a reconstruction signal-to-noise-ratio (SNR) of 31.49dB compared to 20.76dB for the sequential one-frequency setup and 4.02dB for the combined frequency setup. In the noisy setting with 20dB SNR measurements, our method achieves 23.96dB reconstruction SNR compared to 16.69dB for the sequential one-frequency setup and 4.1dB for the combined frequency setup. Note that we provide here a comparison with [14] in lieu of first Born approximation [27] and iterative linearization [28, 29] due to its demonstrated superior performance in the low contrast regime.

In the second experiment, we simulate the scene shown in Figure 5(a) with a domain of size  $1 \times 1\text{m}^2$  and maximum permittivity of 100, discretized on a grid of  $32 \times 32$  pixels. The model contains a water pipe ( $f_{\text{water}} = 100$ ), and a cavity ( $f_{\text{cavity}} = 0$ ). Five trans-receivers placed equidistant on a line  $x = -0.6\text{m}$ . The probing pulse occupies a frequency band from 10 MHz to 800 MHz with a 10MHz step. Additive white Gaussian noise is added to the received measurements to result in 20dB SNR. For the inversion, we set the  $\lambda_j = 1$  for all  $j$  and  $\tau$  to be the TV-norm of the true model. Figures 5(b)–(d) show the incremental reconstruction performance of our proposed method at three recovery stages: 10 MHz, [10, 100] MHz, and [10, 800] MHz. In this high contrast scenario, none of the previous methods were capable of recovering the scene as the objective function is highly nonconvex and the low-frequency reconstruction in Figure 5(b) is too far from the true model. In this noisy very high contrast setup, our proposed method achieves 17.68dB reconstruction SNR compared to 7.4dB for the sequential frequency method [22]

#### 5. CONCLUSION

We developed an incremental frequency inversion framework for the wave-based underground imaging of high-contrast objects. We pose the imaging problem as a nonlinear least-squares problem with total variation regularization and wave-equation constraints. Our incremental frequency setup allows for the recovery of the relative permittivity of extremely high contrast objects embedded in nonhomogeneous media. We demonstrate that our approach achieves better reconstruction quality, around 11dB improvement in SNR, compared to state of the art methods for moderate contrast objects. We also show that our method can recover extremely high contrast objects, such as water with a relative permittivity of 100, where existing techniques fail in the recovery. Future work will feature an analysis of the sensitivity of our approach to the TV bound  $\tau$  as well as adaptively estimating  $\tau$  directly from the data.

## 6. REFERENCES

- [1] S Laurens, JP Balayssac, J Rhazi, G Klysz, and G Arliguie, “Non-destructive evaluation of concrete moisture by gpr: experimental study and direct modeling,” *Materials and structures*, vol. 38, no. 9, pp. 827–832, 2005.
- [2] Simon R Arridge, “Optical tomography in medical imaging,” *Inverse problems*, vol. 15, no. 2, pp. R41, 1999.
- [3] Laurent Sirgue, OI Barkved, J Dellinger, J Etgen, U Albertin, and JH Kommedal, “Thematic set: Full waveform inversion: The next leap forward in imaging at valhall,” *First Break*, vol. 28, no. 4, pp. 65–70, 2010.
- [4] Alan J Witten, John E Molyneux, and Jonathan E Nyquist, “Ground penetrating radar tomography: Algorithms and case studies,” *IEEE Transactions on geoscience and remote sensing*, vol. 32, no. 2, pp. 461–467, 1994.
- [5] Zhen Yuan and Huabei Jiang, “Three-dimensional finite-element-based photoacoustic tomography: Reconstruction algorithm and simulations,” *Medical physics*, vol. 34, no. 2, pp. 538–546, 2007.
- [6] GH Spencer and MVRK Murty, “General ray-tracing procedure,” *JOSA*, vol. 52, no. 6, pp. 672–678, 1962.
- [7] Max Born and Emil Wolf, *Principles of optics: electromagnetic theory of propagation, interference and diffraction of light*, Elsevier, 2013.
- [8] AJ Devaney, “Inverse-scattering theory within the rytov approximation,” *Optics letters*, vol. 6, no. 8, pp. 374–376, 1981.
- [9] Edip Baysal, Dan D Kosloff, and John WC Sherwood, “Reverse time migration,” *Geophysics*, vol. 48, no. 11, pp. 1514–1524, 1983.
- [10] David Colton and Rainer Kress, *Inverse acoustic and electromagnetic scattering theory*, vol. 93, Springer Science & Business Media, 2012.
- [11] Albert Tarantola, “Inversion of seismic reflection data in the acoustic approximation,” *Geophysics*, vol. 49, no. 8, pp. 1259–1266, 1984.
- [12] R Gerhard Pratt, “Seismic waveform inversion in the frequency domain, part 1: Theory and verification in a physical scale model,” *Geophysics*, vol. 64, no. 3, pp. 888–901, 1999.
- [13] Jean Virieux and Stéphane Operto, “An overview of full-waveform inversion in exploration geophysics,” *Geophysics*, vol. 74, no. 6, pp. WCC1–WCC26, 2009.
- [14] Yanting Ma, Hassan Mansour, Dehong Liu, Petros T Boufounos, and Ulugbek S Kamilov, “Accelerated image reconstruction for nonlinear diffractive imaging,” in *2018 IEEE International Conference on Acoustics, Speech and Signal Processing (ICASSP)*. IEEE, 2018, pp. 6473–6477.
- [15] Y Ma, H Mansour, D Liu, PT Boufounos, and US Kamilov, “Nonconvex optimization for diffractive imaging,” in *Mathematics in Imaging*. Optical Society of America, 2018, pp. MW5D–3.
- [16] Yu Sun, Zhihao Xia, and Ulugbek S Kamilov, “Efficient and accurate inversion of multiple scattering with deep learning,” *Optics express*, vol. 26, no. 11, pp. 14678–14688, 2018.
- [17] Alan Richardson, “Seismic full-waveform inversion using deep learning tools and techniques,” *arXiv preprint arXiv:1801.07232*, 2018.
- [18] Mark Schmidt, Ewout Berg, Michael Friedlander, and Kevin Murphy, “Optimizing costly functions with simple constraints: A limited-memory projected quasi-newton algorithm,” in *Artificial Intelligence and Statistics*, 2009, pp. 456–463.
- [19] R-E Plessix, “A review of the adjoint-state method for computing the gradient of a functional with geophysical applications,” *Geophysical Journal International*, vol. 167, no. 2, pp. 495–503, 2006.
- [20] Dong C Liu and Jorge Nocedal, “On the limited memory bfgs method for large scale optimization,” *Mathematical programming*, vol. 45, no. 1-3, pp. 503–528, 1989.
- [21] Stephen Wright and Jorge Nocedal, “Numerical optimization,” *Springer Science*, vol. 35, no. 67-68, pp. 7, 1999.
- [22] C. Borges, A. Gillman, and L. Greengard, “High resolution inverse scattering in two dimensions using recursive linearization,” *SIAM Journal on Imaging Sciences*, vol. 10, no. 2, pp. 641–664, 2017.
- [23] Leonid I Rudin, Stanley Osher, and Emad Fatemi, “Nonlinear total variation based noise removal algorithms,” *Physica D: nonlinear phenomena*, vol. 60, no. 1-4, pp. 259–268, 1992.
- [24] Michael Unser, Julien Fageot, and John Paul Ward, “Splines are universal solutions of linear inverse problems with generalized tv regularization,” *SIAM Review*, vol. 59, no. 4, pp. 769–793, 2017.
- [25] Stephen Boyd, Neal Parikh, Eric Chu, Borja Peleato, Jonathan Eckstein, et al., “Distributed optimization and statistical learning via the alternating direction method of multipliers,” *Foundations and Trends® in Machine learning*, vol. 3, no. 1, pp. 1–122, 2011.
- [26] John Duchi, Shai Shalev-Shwartz, Yoram Singer, and Tushar Chandra, “Efficient projections onto the  $l_1$ -ball for learning in high dimensions,” in *Proceedings of the 25th international conference on Machine learning*. ACM, 2008, pp. 272–279.
- [27] M. Born and E. Wolf, *Principles of Optics*, chapter Scattering from inhomogeneous media, pp. 695–734, Cambridge Univ. Press, 7 edition, 2003.
- [28] K. Belkebir, P. C. Chaumet, and A. Sentenac, “Superresolution in total internal reflection tomography,” *J. Opt. Soc. Am. A*, vol. 22, no. 9, pp. 1889–1897, September 2005.
- [29] P. C. Chaumet and K. Belkebir, “Three-dimensional reconstruction from real data using a conjugate gradient-coupled dipole method,” *Inv. Probl.*, vol. 25, no. 2, pp. 024003, 2009.